



Spatiotemporal scale-dependent effects of urban morphology on meteorology: A case study in Beijing using observations and simulations

Nana Li^{a,*}, Jiaxi Yang^a, Xiaoxu Tang^b

^a Institute of Urban Meteorology, China Meteorological Administration, Beijing, 100089, China

^b Beijing Key Laboratory of Urban Spatial Information Engineering, Beijing Institute of Surveying and Mapping, Municipal Commission for City Planning and Resources Management, Beijing, 100038, China

ARTICLE INFO

Keywords:
2D/3D urban morphology
Urban meteorology
Scale effect
In-situ observation
WRF simulation

ABSTRACT

Urban morphology has a great impact on urban meteorology, but the scaling effects in the underlying relationships have seen little research. In this work, the controls of building and vegetation morphology on urban meteorology at different spatial (30 m, 90 m, 300 m, 500 m, 1 km) and temporal (diurnal, seasonal) scales are explored, using in-situ observations and WRF (Weather Research and Forecast) modeling. The random forest method is employed to derive the importance of morphological indicators for meteorology, based on in-situ observations from weather stations. This work reaches the following conclusions. (1) Morphological factors have the largest impacts at 30-m scale, and are the strongest influences on air temperature (T_a), wind speed (WS) and relative humidity (RH). The sky view factor (SVF) is the most important of these factors at the 30-m scale. Vegetation strongly affects T_a and RH in summer at scales of >90 m. (2) The main indicators during daytime and night-time are different: vegetation has a more impact on T_a during the night than during the day in summer, while SVF is the main factor controlling T_a at night during winter. Morphology has greater influence on diurnal variations in T_a at scales of <100 m. (3) The WRF simulation is consistent with observations and reveals that building height is the most important indicator for WS. This is because building height affects the roughness length for momentum (Z_{0m}), which is the main factor influencing WS. This work can help in urban planning, to improve the urban thermal and wind environment.

1. Introduction

With economic growth and increasing population, urban land is under high demand. Besides horizontal urban expansion, urban areas are also growing rapidly upwards. The diversity of urban surface components and the greater variety in building heights introduce increasingly complex urban surfaces. The 3D urban structure alters the surface dynamics and heat transfer processes, thereby influencing urban meteorology and climate [1]. Previous studies have shown that the 3D urban morphology has a stronger impact on urban microclimate than 2D morphology [1,2]. Urban surfaces have a lower sky view factor and lower surface albedo, which trap and store more solar radiation and thus increase urban heating [3]. Also, 3D urban surfaces have larger surface areas than natural surfaces, that will absorb more energy during daytime, and owing to the higher heat capacity of impervious surfaces, the stored energy is released during the night. Consequently, urban surfaces affect air temperature more strongly at night [4,5]. Besides temperature,

3D urban surfaces have a greater surface roughness, which influences the urban wind [6].

At present, numerical modeling and in-situ observations are the main methods for studying the impact of urban morphology on microclimate. Some studies have evaluated the high-resolution urban morphology parameters within the WRF (Weather Research and Forecast) model in urban meteorology simulations. For example, Zhang et al. (2020) [7] employed morphology parameters from NUDAPT (National Urban Database and Access Portal Tool) instead of the defaults; Sun et al. (2021) [8] and He et al. (2019) [9] used real morphology parameters from building data, and showed the new parameters could improve air temperature and wind speed simulation. Compared to the WRF- a meso-scale model, CFD (computational fluid dynamics) models have advantages for microscale urban climate simulations. For example, some studies showed that building height is the most influential factor for outdoor air temperature, when employing ENVI-Met software [10] and RANS (Reynolds-averaged Navier-Stokes equations) [11]. Yu et al.

* Corresponding author.

E-mail address: nqli@ium.cn (N. Li).



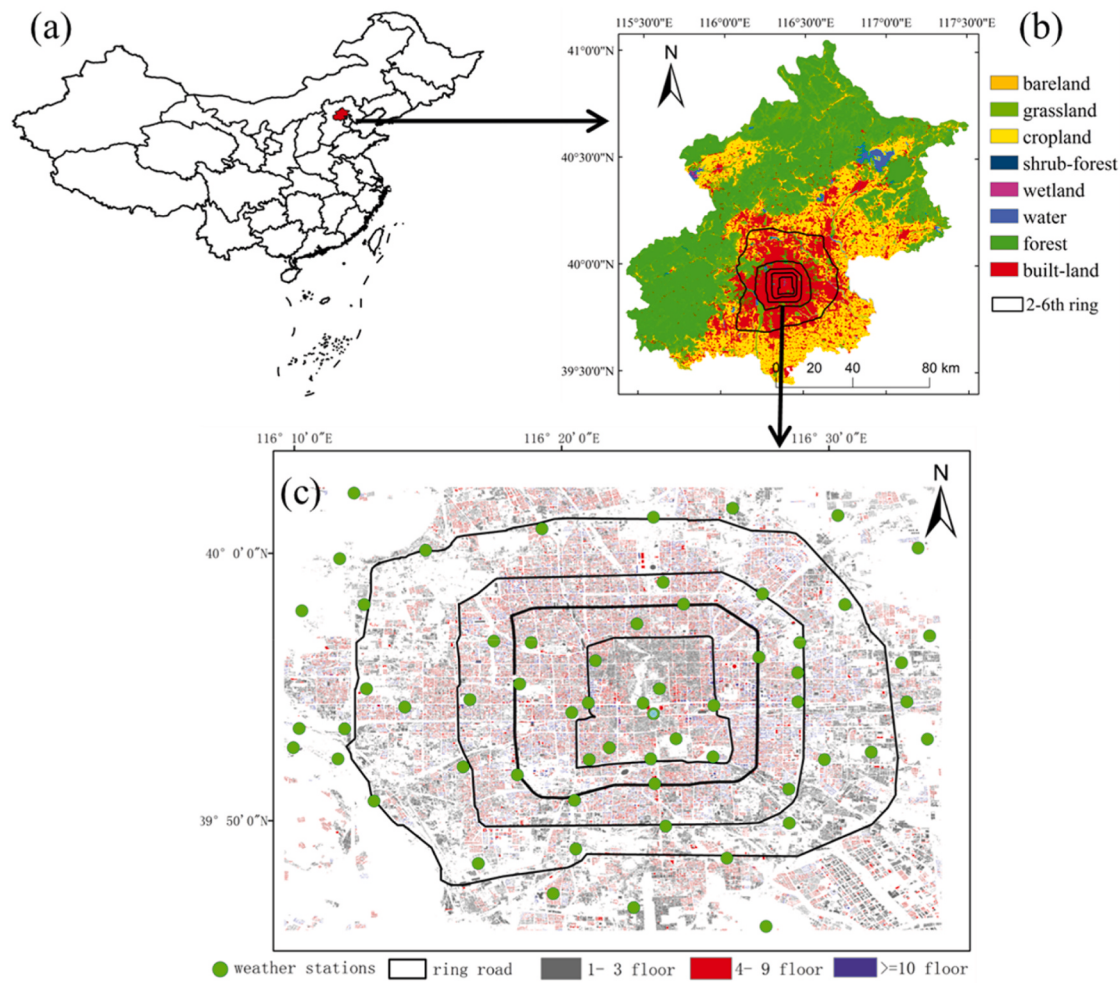


Fig. 1. Study area of Beijing, China: (a) location of Beijing in China, (b) landcover types in Beijing in 2020, (c) automatic weather stations and building footprints within the 5th ring of Beijing in 2018.

(2020) [12] observed diurnal variations in outdoor air temperature in a campus of Singapore and revealed that sky view factor and building wall area were the strongest influences on morning and afternoon air temperatures, respectively. Tong et al. (2018) [13] showed that building height and street width had greater impacts on daily maximum air temperature in summer than in winter. Liu et al. (2020) [6] explored the relationship between wind speed and building morphology at 500 m spatial resolution, and showed that sky view factor, floor area ratio and frontal area index have the greatest influences on wind speed. Cao et al. (2021) [14] studied the spatial and seasonal variations of building morphology and urban environment in Beijing, using linear regression. They showed that 3D morphology had a stronger influence on the urban environment than a 2D representation. In addition, some studies employed local climate zones (LCZs) to explore effects of urban morphology on urban climate and also revealed the important impact of 3D morphology [15–19].

Studies based on field measurements are usually more accurate than simulations [20,21]; however, most previous studies have analyzed relationships with linear regression, which is not suitable for exploring the complex nonlinear relationship between morphology and meteorology. In addition, some studies focus on only building morphology, and neglect the influence of vegetation [6,14]. Numerical models provide helpful tools in this respect, for example CFD model is a favorable tool

for urban climate studies at a microscale (the domain size is usually less than 1 km and the model resolution is less than 1 m). However, expanding the simulation domain can significantly increase the computational cost. Thus, most CFD simulations are limited to a spatial extent of $2 \times 2 \text{ km}^2$ [22]. Although the resolution of the WRF model is not so high, it is a good choice for city-scale simulations at a mesoscale (the domain size is usually less than 100 km).

The studies reviewed above demonstrate that the impacts of urban morphology on meteorology are relevant across spatial and temporal scales. However, studies of the scale-effect remain limited, whether using numerical models or field measurements. To address this gap, we note that machine learning is an excellent tool for solving nonlinear relationships. To take advantage of that approach, this study employs the random forest method to explore the association between urban morphology and urban microclimate at different spatial (30 m–1 km) and temporal (diurnal, seasonal) scales. Building and vegetation morphologies, and dozens of weather stations, are included. Finally, the WRF model coupled with these real urban morphologies is used to reveal the physical processes through which the morphology affects urban microclimate. According to some previous studies, urban morphology strongly affects wind speed, but not air temperature using numerical models [23,24]. Therefore, here only the wind speed is simulated by WRF model.

2. Methodology

2.1. Study area

Beijing ($39^{\circ}28' - 41^{\circ}05'N$, $115^{\circ}25' - 117^{\circ}35'E$), the capital of China, is located on the North China Plain. The city has an area of about 16410 km^2 and population of 22 million. It includes diverse land and terrain types, and has an average elevation of approximately 43.5 m (Fig. 1b). The city has a typical continental monsoon climate with a mean annual air temperature of $10-12^{\circ}\text{C}$ and mean annual precipitation of $450-550 \text{ mm}$. This study is focused on the central area of Beijing (roughly within the 5th ring road), in an area of about 667 km^2 covered almost entirely by buildings (Fig. 1c). Most buildings have 1–3 floors, followed by 4–9 floors and finally ≥ 10 floors.

2.2. 2D/3D urban morphology indicators

Nine indicators were selected, including seven building indicators and two vegetation indicators. The vegetation indicators were normalized difference vegetation index (NDVI) and fractional vegetation cover (FVC), which were derived from the Gaofen-1 (GF-1) satellite and were available with 16-m spatial resolution and 10-day temporal resolution in 2018. Both products can be freely downloaded from the “Science Data Bank” (<https://www.scidb.cn/en/detail?dataSetId=841373295210135552>) [25,26]. The seven building indicators were mean building height (BH), mean building density (BD), building surface area to plan area ratio (λ_B), floor area ratio (FAR), sky view factor (SVF), frontal area index (FAI), and building shade (BS). The building indicators were required in gridded format, but were obtained from Baidu Map as vector-format building footprint and height data. Therefore, the vector data were firstly converted to raster data with a spatial resolution of 10 m, before calculating the gridded building indicators.

This study calculated the indicators at spatial scales of 30 m, 90 m, 300 m, 500 m and 1 km, based on the 10 m building data. Meanwhile, the seasonal average and season-hourly indicators were also calculated, e.g. seasonal FAI and hourly BS. The following relationships were used.

(1) Mean building height (BH)

$$BH = \frac{\sum_{i=1}^n A_i H_i}{\sum_{i=1}^n A_i} \quad (1)$$

where A_i and H_i are the i th building plan area and height, and n is the total number of buildings in the target pixel.

(2) Mean building density

$$BD = \frac{\sum_{i=1}^n A_i}{A_{pixel}} \quad (2)$$

where A_{pixel} is the target pixel size, and other symbols follow Eq. (1).

(3) Building surface area to plan area ratio (λ_B)

$$\lambda_B = \frac{\sum_{i=1}^n (A_{r,i} + A_{w,i})}{A_{pixel}} \quad (3)$$

where $A_{r,i}$ and $A_{w,i}$ are roof and total wall areas of the i th building, and other symbols are same as above.

(4) Floor area ratio (FAR)

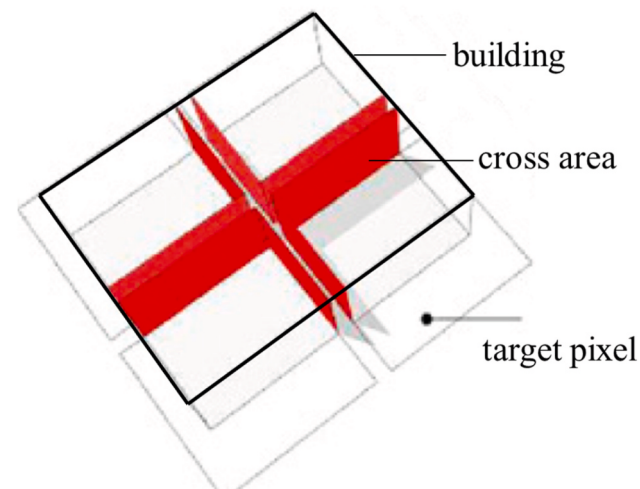


Fig. 2. A building is divided into four grid cells, the red area is the cross sections. (For interpretation of the references to colour in this figure legend, the reader is referred to the Web version of this article.)

$$FAR = \frac{\sum_{i=1}^n A_i \times N_i}{A_{pixel}} \quad (4)$$

where N_i is the number of floors in building i , and other symbols are same as above.

(5) Sky view factor (SVF)

$$SVF = 1 - \frac{\sum_{i=1}^m \sin \gamma_i}{m} \quad (5)$$

where γ_i is the influence of terrain elevation angle of the i th azimuth angle (with units of radians), and m is the number of azimuths ($m = 36$ in this study). SVF = 0 indicates the sky is totally covered, while SVF = 1 indicates the sky is completely unobstructed [27].

(6) Frontal area index (FAI)

FAI (λ_f) is the ratio of projected building area to the target plane area, for a specific wind direction [28].

$$\lambda_{f(\theta)} = \frac{A(\theta)_{proj}}{A_{pixel}} \quad (6)$$

$$\lambda_f = \sum_{n=1}^{16} \lambda_{f(\theta)} \cdot P(\theta) \quad (7)$$

where $\lambda_f(\theta)$ is the frontal area index at wind direction θ , and λ_f is the frontal area index for all wind directions; $A(\theta)_{proj}$ is the projected building area in wind direction θ ; $P(\theta)$ is wind frequency in direction θ . Sixteen directions θ were used in this study: north (central angle of 0°), north-north-east (22.5°), north-east (45°), east-north-east (67.5°), east (90°), east-south-east (112.5°), east-south (135°), south-south-east (157.5°), south (180°), south-west-south (202.5°), south-west (225°), west-south-west (247.5°), west (270°), west-north-west (292.5°), north-west (315°), and north-north-west (337.5°). $P(\theta)$ is calculated based on the observed wind direction data from weather stations in 2018 in Beijing.

FAI can be derived based on vector or raster data, using different calculation approaches. When using vector data, the calculated FAI is appropriate for a larger spatial scales, e.g. $>200 \text{ m} \times 200 \text{ m}$. However,

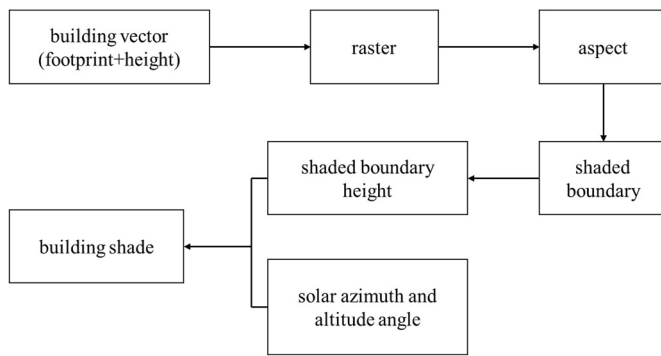


Fig. 3. The flowchart for building shade calculation based on the building data.

Table 1
WRF simulation cases with different urban morphology settings.

	Default case	Case 1	Case 2	Case 3	Case 4
Parameter settings	No morphology	Only building density	Only building height	Only surface area ratio	Only frontal area index

the raster approach can obtain FAI at any resolution. This study used building raster data to calculate FAI at 30 m, 90 m, 300 m, 500 m, 1 km scales, respectively. In addition, we also considered the situation in which an individual building is divided by the raster pixel (Fig. 2).

(7) Building shade (BS)

The hourly building shading was calculated based on the building footprint and height data, using ArcGIS and Python. Firstly, the building vector data were converted to raster data and then used to calculate building aspect. Secondly, building aspect was used to select the shaded building boundary, using $\sim[A-90, A+90]$ with solar azimuth A . The building shade was indicated by the shaded building boundary. Thirdly, by combining building height and shaded building boundary, the shaded boundary height was obtained. Finally, combined with shaded boundary height and the solar azimuth and altitude angles, the building shade could be calculated by the “Hillshade” function in ArcGIS (Fig. 3).

2.3. In-situ meteorological observations

The hourly meteorological data in 2018 and 2019 were derived from 61 automatic weather stations covering the building footprint data in this study (Fig. 1c). The stations are operated by the Beijing Meteorological Service (<http://bj.cma.gov.cn/>) and all the station data are quality-controlled. Air temperature (T_a), wind speed (WS) and relative humidity (RH) were used in this study. Seasonal averages and seasonal-hourly data were calculated for each site. Spring was defined as March–May 2018, summer as June–August 2018, autumn as September–November 2018, and winter December 2018–February 2019.

2.4. Spatial scale quantified by buffer zones

The urban morphology indicators were extracted from circular buffer zones with diameters of 30 m, 90 m, 300 m, 500 m, 1 km, respectively, each having a weather station at the center of the circle. Compared to the approach using weather station data within a grid box, the buffer zone approach could provide more representative morphology variables at different spatial scales. The relationships between urban morphology and urban microclimate in different buffer zones (different spatial scales) were then analyzed.

2.5. Importance of morphological factors

The random forest (RF) method was used here to evaluate the importance of urban morphological factors for urban microclimate. RF integrates multi-decision trees and is an extension of a bagging algorithm, with the advantage of high accuracy, high robustness, and insensitivity to multi-collinearity [29,30]. RF is an efficient and robust method for feature selection, which can handle high-dimensional input variables, noisy data, missing data, and outliers. RF can exploit nonlinear relationships, and has been widely used for regression [31, 32]. It utilizes a bootstrap approach to select training data, and always about 37% of samples are not selected (these are called ‘out-of-bag’ or OOB samples). The OOB samples are used as test data, to ensure the RF method cannot use training samples as test samples. The OOB score (R^2) is used to evaluate the RF model (Eq.(8)–(10)). Each tree has one R^2 value, and the average of all R^2 values of all decision trees quantifies the R^2 of the RF model. The OOB error is $1-R^2$.

In general, there are two approaches for feature importance evaluation using the RF method. One is based on the mean decrease in impurity, and other is based on mean decrease in accuracy. The biggest advantage of the impurity-based method is its speed of computation, as it is only implemented in the training stage. However, a drawback of the impurity-based method is that in the case of correlated features it can select one feature and neglect the importance of another, which can lead to wrong conclusions. The accuracy-based method is actually a permutation-based method, which randomly shuffles each feature (i.e., one feature is changed and the other features are kept unchanged), and then computes how the change affects the RF’s performance. The accuracy-based method can overcome the drawbacks of the impurity-based method, but it is time consuming because it is applied to both the training and test stages. The feature which impacts the RF performance (change of OOB error) most is identified as the most important feature.

In this study, we used the accuracy-based feature importance to analyze the relative influence of input variables on urban microclimate. All nine urban morphology indicators were used as input variables. Testing showed little further improvement in OOB score with more than 500 trees, so 500 trees were considered sufficient for this study (ntree = 500). The importance values were normalized to the range 0–1 in this study, for the purpose of comparative analysis. The corresponding formulae are as follows.

$$R^2 = 1 - \frac{u}{v} \quad (8)$$

$$u = \sum_{i=1}^N (f_i - y_i)^2 \quad (9)$$

$$v = \sum_{i=1}^N (y_i - \bar{y})^2 \quad (10)$$

where R^2 is the OOB score, u/v is the OOB error, N is the number of samples, f and y are the simulated and true values, and \bar{y} is the mean of the true values.

2.6. WRF simulation

WRF model version 4.3.3 coupled with BEP was used for WS simulation in this study. The physical parameterization schemes used here include the YSU boundary layer scheme [33], RRTMG longwave and shortwave radiation scheme [34], Thompson microphysical process [35], Kain-Fritsch cumulus parameterization scheme [36], and Noah land surface model [37]. WRF configured with three one-way nested domains centered at 39°N, 116°E; the innermost domain included the entire Beijing urban area. The horizontal resolutions were 9 km (D01 outer), 3 km (D02 middle), and 1 km (D03 inner), and the grid size of

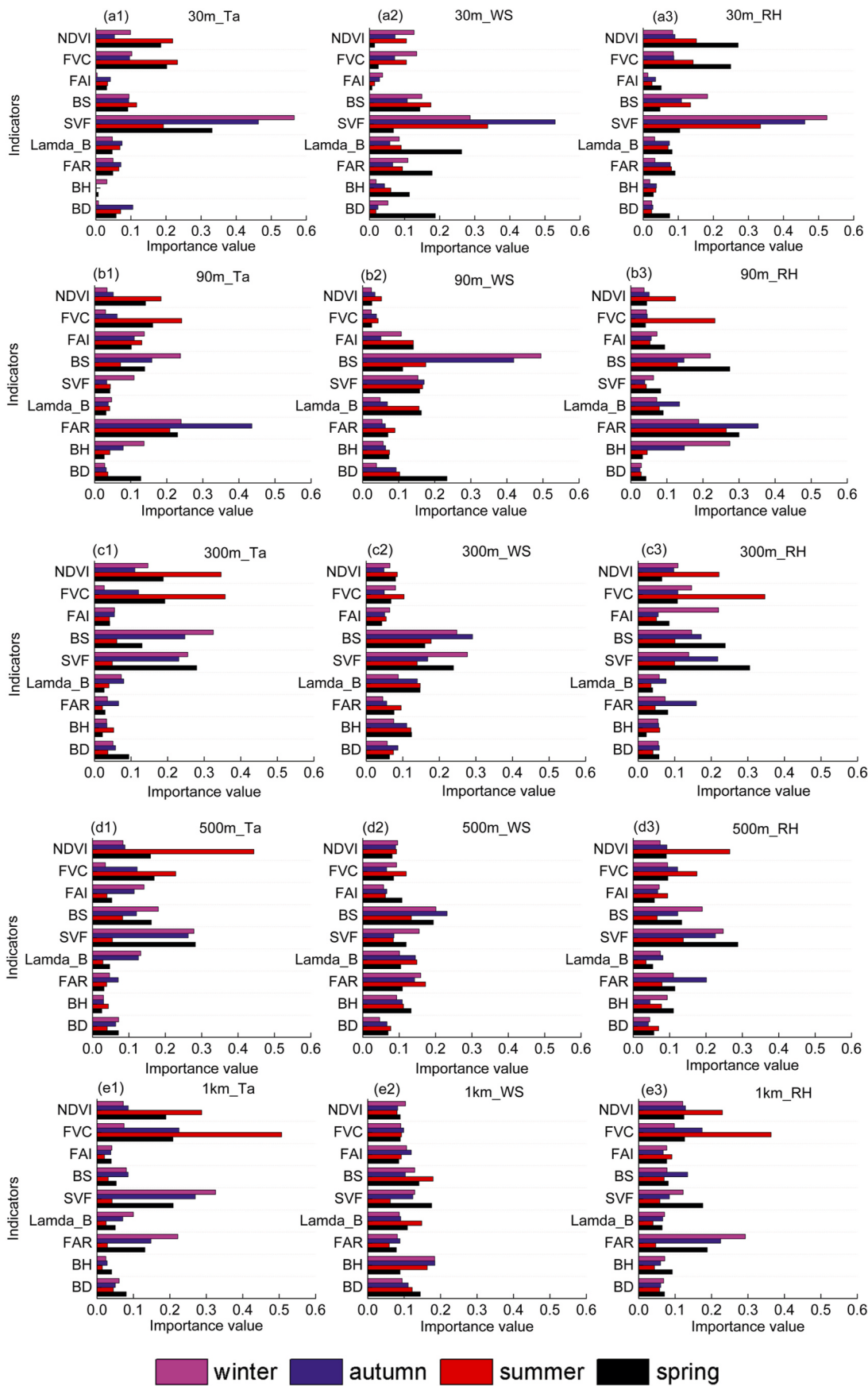


Fig. 4. The relative importance of morphological indicators for seasonal microclimates at different spatial scales: (a1–a3) at 30 m scale, (b1–b3) at 90 m scale, (c1–c3) at 300 m scale, (d1–d3) at 500 m scale, and (e1–e3) at 1 km scale.

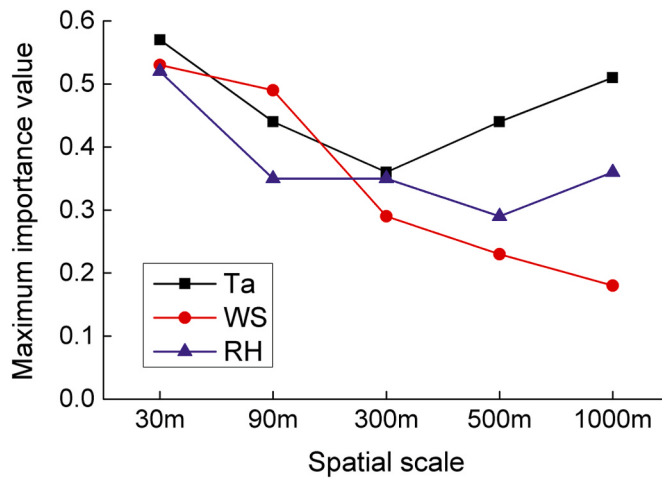


Fig. 5. The variation of the annual maximum importance of morphological indicators at different spatial scales.

Table 2

The maximum importance of morphological indicators at different scales, in summer and winter of 2018.

	Parameter	30 m	90 m	300 m	500 m	1 km
Summer	T _a	FVC	FVC	FVC	NDVI	FVC
	RH	SVF	FAR	FVC	NDVI	FVC
	WS	SVF	BS	BS	FAR	BS
Winter	T _a	SVF	FAR, BS	BS	SVF	SVF
	RH	SVF	BH	FAI	SVF	FAR
	WS	SVF	BS	SVF	BS	BH

D03 was 64×64 . In the vertical, 38 levels were used from the surface to 50 hPa. The initial and boundary conditions were obtained from the fifth generation ECMWF atmospheric reanalysis data (ERA5) with 0.25° spatial resolution.

Five experiments were carried out to investigate the impact of morphology factors on WS simulation (Table 1). For the purpose of reducing the impact of weather conditions (e.g. rainy and windy conditions) on the simulation, three sunny days in October were chosen for the simulation (1–3rd October). In general, the weather conditions are relatively stable during October in Beijing. As urban morphology has more impact on wind speed simulation than on other meteorological elements, the roughness length for momentum (Z_{0m}) was considered the main factor influencing wind speed. Therefore, Z_{0m} in WRF as presented by Macdonald et al. (1998) [38] (Eqs. (11) to (12) below) was employed here to investigate how the urban morphologies affect wind speed.

$$\frac{Z_d}{Z_H} = 1 + \alpha^{-\lambda_p} (\lambda_p - 1) \quad (11)$$

$$\frac{Z_{0m}}{Z_H} = \left(1 - \frac{Z_d}{Z_H} \right) \exp \left\{ - \left[0.5\beta \frac{C_D}{k^2} \left(1 - \frac{Z_d}{Z_H} \right) \lambda_F \right]^{-0.5} \right\} \quad (12)$$

Here Z_d is zero-plane displacement length, Z_H is building height, Z_{0m} is roughness length for momentum, λ_p is building density, λ_F is frontal area index, k is von Karman's constant ($k = 0.4$), and α and β are empirical coefficients. Here we use $\alpha = 4.43$ and $\beta = 1.0$ as recommended by Ref. [38] for staggered arrays of cubes based on wind tunnel data, C_D is a drag coefficient, with $C_D = 1.2$ recommended by Macdonald et al. (1998) [38]. Grimmond et al. (1998) and Liu et al. (2016) [39,40] used other morphological indicators to estimate FAI, for example building density. In this study, we calculated FAI using the real building data, based on the FAI definition above.

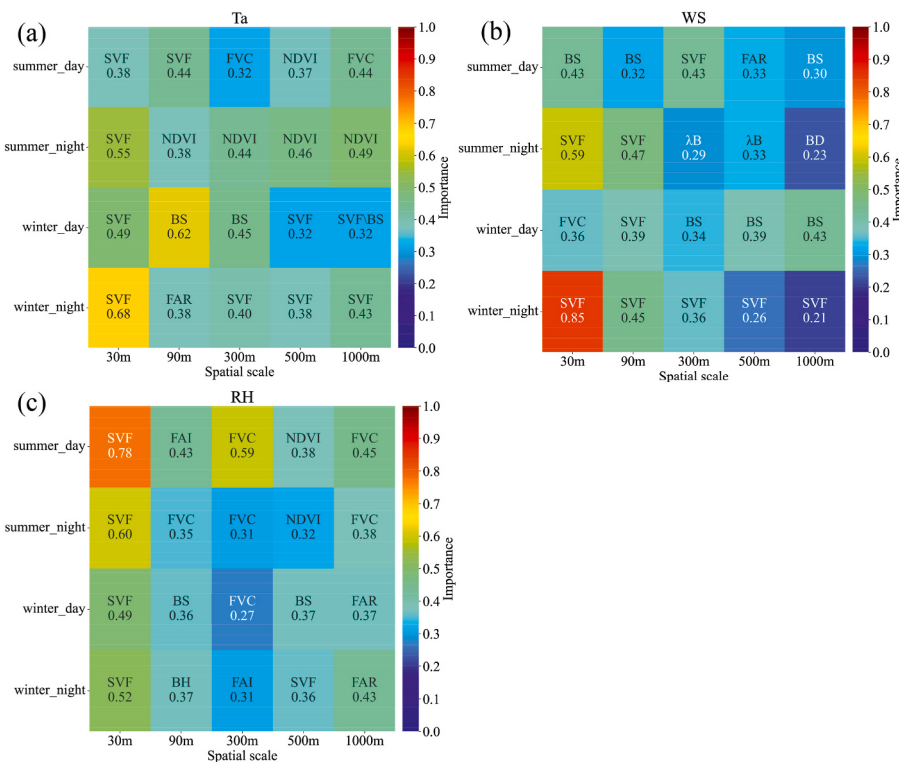


Fig. 6. The maximum importance and its corresponding indicators at different spatial scales, during daytime and night-time in summer and winter of 2018 for (a) T_a , (b) WS , (c) RH .

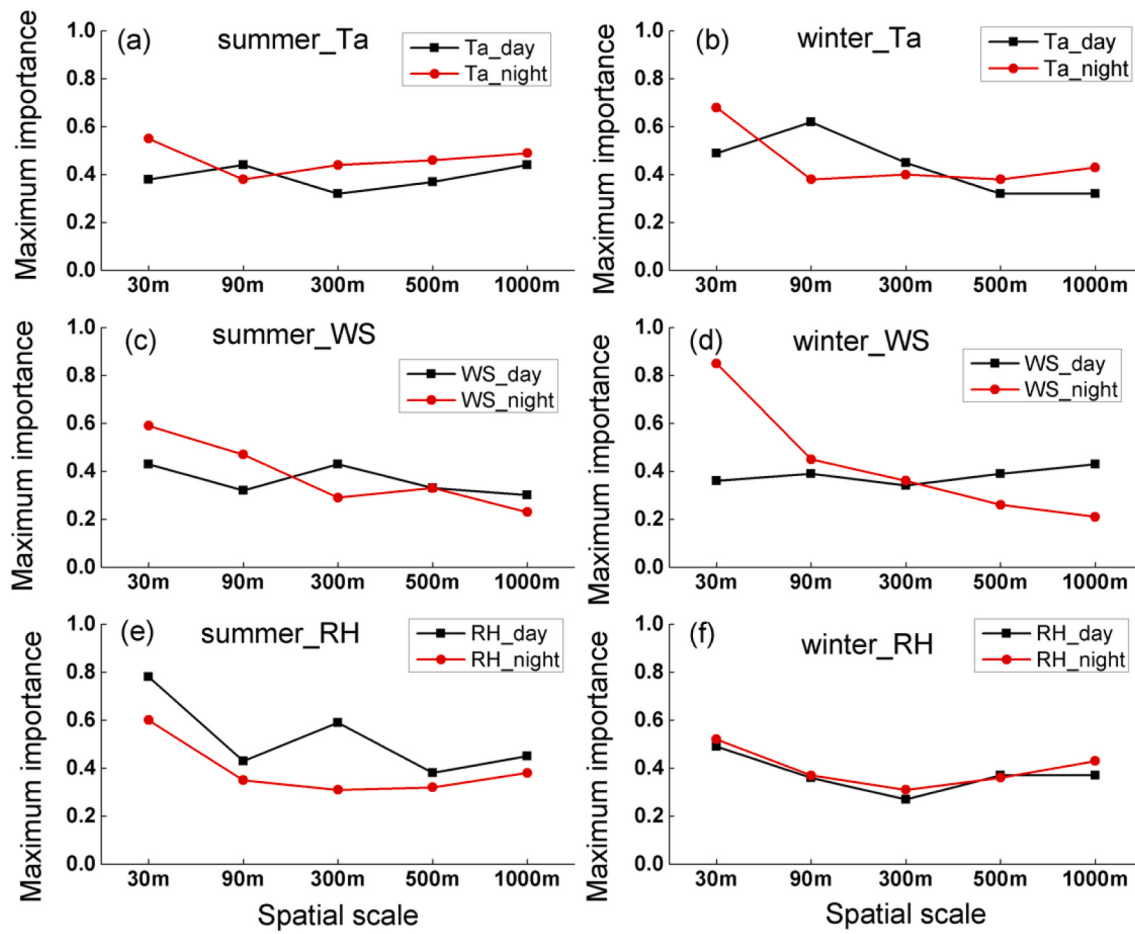


Fig. 7. The variation of the maximum importance of morphology indicators during daytime and night-time in summer and winter, 2018, at different spatial scales.

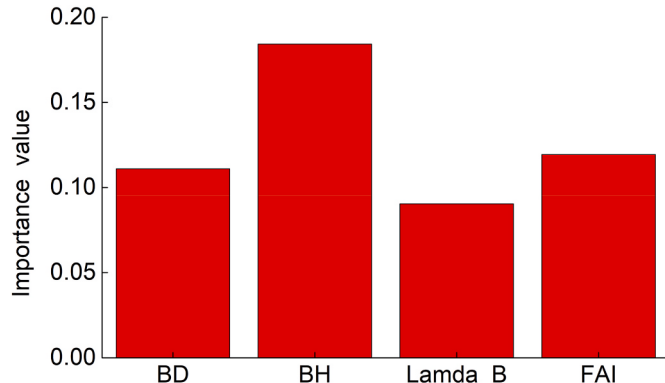


Fig. 8. The importance values of the four indicators in the RF model using 61 weather stations at 1-km scale, during 1–3rd October 2018.

3. Results and discussion

3.1. Spatial and seasonal scale effects of morphologies on microclimate

The importance of indicators varies with both spatial and seasonal scale. For T_a , SVF is the most influential factor at 30 m, while FAR, FVC, NDVI, and FVC are the most influential factors at 90 m, 300 m, 500 m and 1 km, respectively, on the annual time scale (Fig. 4). At 30 m scale, SVF is the most influential factor on T_a in winter, while FVC is the most influential factor on T_a in summer (Fig. 4).

We next select the maximum importance values of indicators at

different scales (Fig. 5). For WS, the importance decreases with increasing length scale, indicating that the impact of urban geometry on WS is more significant at a smaller spatial scale. However, for T_a , the importance first decreases to minimum of 0.36 at 300 m, then increases. For RH, the minimum importance (0.29) is at 500 m. Nevertheless, the importance at 30 m is still larger than that at 1 km for both T_a and RH. In general, the importance is maximum at 30 m for T_a , WS and RH, which shows the urban geometry has more influence on microclimate at 30 m scale than at other longer scales.

The maximum values of importance in summer and winter are next considered separately (Table 2). For T_a , in summer, vegetation (FVC, NDVI) is the most important factor at any spatial scale, while in winter, there is no vegetation, and the role of building morphology becomes more important (with SVF and BS as the main factors).

The underlying surface mainly affects T_a by changing the turbulent exchange coefficient between surface and surface air. SVF is a competitive indicator, associated with building height and density which are both directly related to the turbulent exchange coefficient. The influence of BS on cooling depends on shading. The effect of urban geometry on WS is mainly through changes in roughness length for momentum (Z_{0m}). There are few trees within the 5th ring of Beijing, so the building height and density are the main factors affecting Z_{0m} . SVF and BS, related to both building height and density, are the main indicators for WS in summer and winter. In theory, the area of BS is affected by building height and density. For RH, vegetation (FVC) is the most important factor in summer due to its influence on transpiration. Interestingly, SVF is the main factor in summer and winter at 30 m scale, for each of T_a , WS and RH.

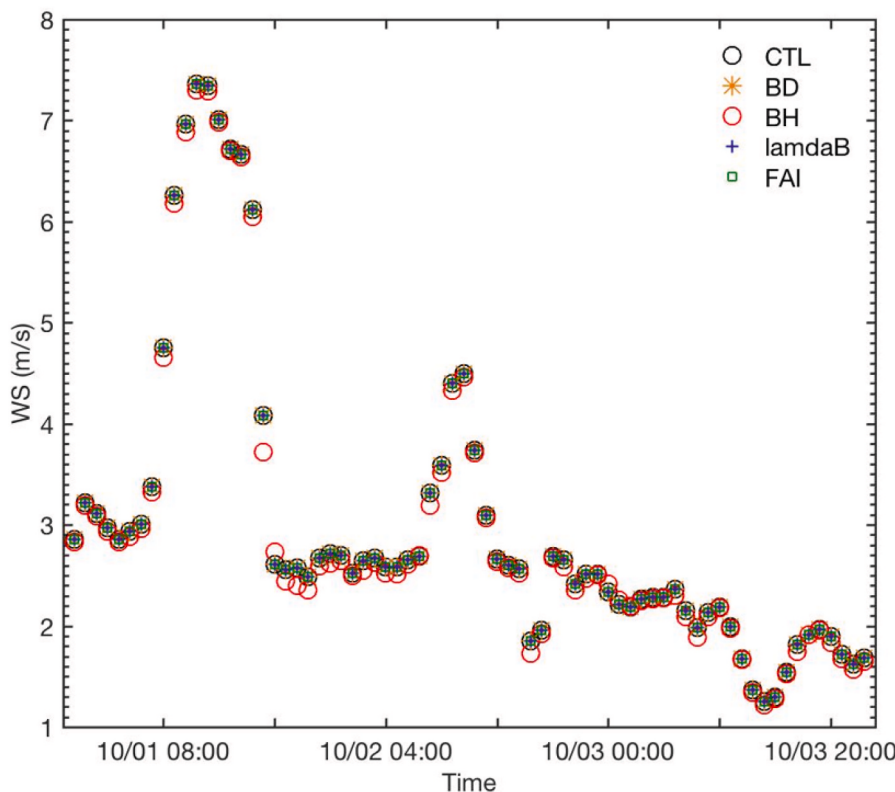


Fig. 9. Wind speed simulations with and without morphology indicators at 61 weather stations simulated by the WRF model at 1-km scale, during 1–3rd October 2018. ‘CTL’ is without morphology, BD, BH, λ_B and FAI are simulations with building density, building height, building surface area ratio and frontal area index, respectively.

3.2. Spatial and diurnal variability in the effects of morphologies on microclimate

Day and night are divided according to the solar altitude angle (h). If $h > 0$, it is daytime; if $h < 0$, it is night-time. Thus, the summer day is 5:00–19:00 and summer night is 20:00–4:00; the winter day is 7:00–17:00 and winter night is 18:00–6:00. The main factors influencing daytime and night-time T_a , WS and RH vary for different scales (Fig. 6). For T_a , vegetation is the main factor during summer days and nights at scales of >300 m, and in summer, vegetation is more important at night than during the day (Fig. 6a). In winter, as vegetation has died back, building morphology becomes the main factor affecting T_a , with greatest influences from SVF at night and SVF and BS during the day (Fig. 6a). SVF influences T_a more at night than during the day. For WS, in general BS is the main factor during daytime in summer and winter, switching to SVF and λ_B during the night (Fig. 6b). The three factors are all related to building height and density, which affect Z_{0m} . In winter night-time, SVF is a strong influence on WS at all scales. For RH, the important factors are generally similar to those of T_a , because T_a and RH are strongly correlated.

For T_a the important factors are most influential at the 30-m scale during the night and at the 90-m scale during the day (Fig. 7 a–b). Therefore, the urban morphology is most important for T_a at scales <100 m. For WS the influence of important urban morphological factors decreases with increasing scale at night, while there is no notable scaling effect during the day (Fig. 7 c–d). For RH, the urban morphology has the largest importance at 30 m scale in both summer and winter, and during both day and night (Fig. 7 e–f).

3.3. Comparison of observations and WRF simulations

The simulation and observation results are consistent, and show that

the building height is the most important factor for WS (Figs. 8 and 9). The reference simulation of WS with no morphologies (CTL) is compared to WS simulated with BD, BH, λ_B and FAI (Fig. 9). The differences between the simulations with BD, λ_B and FAI are small, however, WS with BH is a little different with other simulations. BH may increase surface resistance, which would then reduce WS.

We next investigate why BH mostly influences WS by analyzing the relationship between Z_{0m} and the morphological factors (Fig. 10). Z_{0m} increases exponentially with increasing BH (Fig. 10a), similarly to FAI (Fig. 10c). Z_{0m} first increases but then decreases with increasing BD (Fig. 10b). In regions where the mean building height near weather stations is below 20 m, the corresponding Z_{0m} is less than 2 m. Although FAI values are relatively discretely distributed when compared to those of BH, in regions where the FAI near weather stations is less than 0.1 the corresponding Z_{0m} is also less than 2 m. In regions where the building density at weather stations is mostly greater than 0.3, the corresponding Z_{0m} is less than 1 m. Nevertheless, the effect of BH and FAI is comparable for Z_{0m} (Fig. 10). WS is also influenced by zero-plane displacement height, except for Z_{0m} , which is directly proportional to BH [9]. Therefore, BH has a greater impact on WS at scale of 1 km, consistent with Cao et al. (2021) and Hanna et al. (2002) [14,41].

4. Limitations and future work

There are still some limitations of this work, as described below.

First, only the “mean decreasing accuracy” method in the RF model is used in important-factor studies. Multiple methods should be integrated to study the importance, e.g. SHAP (Shapley Additive exPlanations) [42], mutual information [31], and others.

Second, there is a lack of 3D vegetation morphology, e.g. tree height, vegetation volume, LAD (leaf area density), etc. Although there is an open global forest canopy height dataset with 30-m resolution, based on

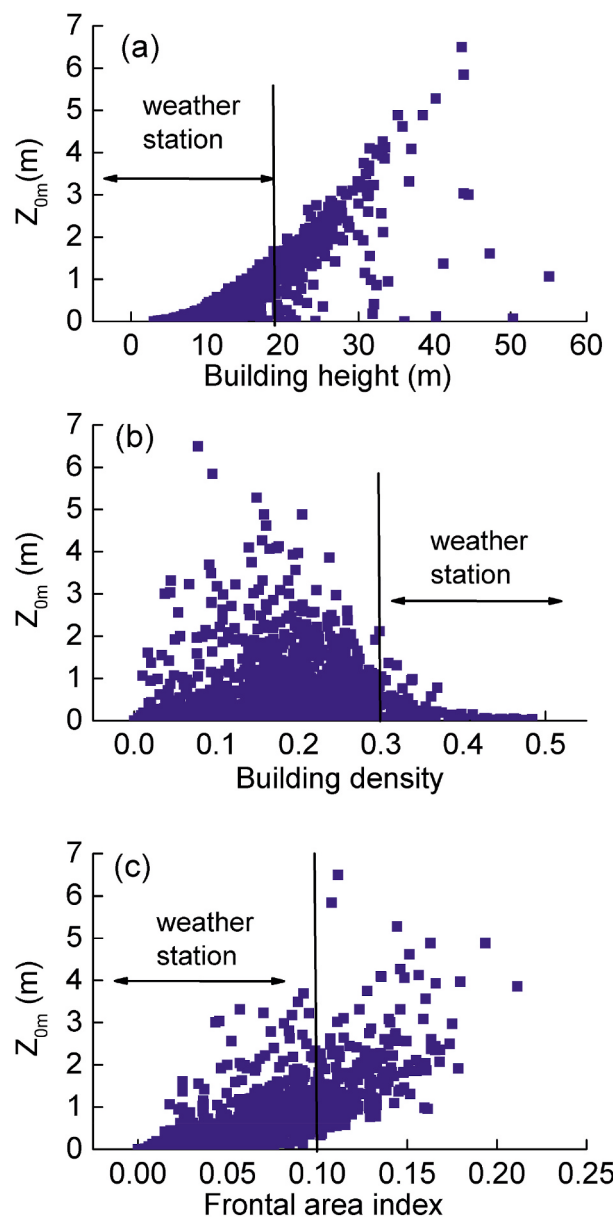


Fig. 10. The relationship between Z_{0m} and morphological indicators (a) BH, (b) BD, (c) FAI, respectively.

integrated GEDI and Landsat data [43], this product may have important uncertainties when used in urban applications (Dr. Potapov, pers. comm.). A ground-based 3D laser scanning imaging system could obtain vegetation morphology more accurately, but would be impractical at the city scale. The combination of a ground-based 3D laser scanning observation and satellite Lidar data could be an effective approach for quantifying 3D vegetation morphology at the city scale [44].

Finally, the WRF model is a mesoscale meteorological model which is mostly utilized for simulation at a coarse resolution. Integration of a microscale model (e.g. CFD) and the WRF model could help with the evaluation of the relationship between urban morphology and meteorology from meter to kilometer scales [45].

5. Conclusions

This study explored the impact of urban morphology on microclimate in Beijing, at spatial scales of 30 m, 90 m, 300 m, 500 m, and 1 km, and at diurnal and seasonal temporal scales, using the random forest

method and WRF model. The building and vegetation morphologies were retrieved from Baidu Map and Gaofen-1 satellite data in 2018, respectively. Urban microclimate variables (T_a , WS, RH) were acquired from weather stations in 2018 and 2019. The random forest method was able to provide quantitative measures of the importance of morphological indicators, thereby demonstrating its value for improving understanding of associations between urban form and urban meteorology. The findings of this study are follows.

- (1) The importance of the main morphological indicators for annual-scale WS decreases with increasing spatial scale, while the importance first decreases and then increase for T_a and RH. The greatest importance of morphological values is at 30 m scale for each of T_a , WS and RH; therefore, the morphology has the greatest impact at 30 m than at other scales. SVF is the most influential factor at 30 m scale. Vegetation strongly affects T_a and RH in summer at scales >90 m. SVF and BS are the most important factors influencing WS in both summer and winter; both factors are related to building height and density and thus affect WS via Z_{0m} .
- (2) The main factors influencing urban microclimate vary between day and night. Vegetation impacts T_a more during the night than during the day in summer, and SVF is more important at night than during the day in winter. The greatest influence on T_a is at 30 m scale at night and at 90 m scale during the day, showing that the role of morphology is significant for T_a at scales of <100 m.
- (3) The WRF simulation is consistent with observations, and shows building height is the most important factor influencing WS. This is because the Z_{0m} associated with buildings is relatively large. In addition, building height affects zero plane displacement height directly, which is another factor influencing WS.

Further to our results above, there are also some limitations. Other methods, e.g. SHAP or mutual information, should be integrated with the “mean decreasing accuracy” used in this study to explore the indicator importance. The 3D vegetation morphology (e.g. vegetation volume, leaf area density et al.) should be included, by integrating field measurements and satellite Lidar data. Moreover, a CFD model could be employed to explore the physical processes driving microscale urban meteorology.

CRediT authorship contribution statement

Nana Li: Writing – original draft, Methodology, Funding acquisition, Conceptualization. **Jiaxi Yang:** Writing – review & editing, Visualization, Formal analysis. **Xiaoxu Tang:** Writing – review & editing, Resources, Data curation.

Declaration of competing interest

The authors declare that they have no known competing financial interests or personal relationships that could have appeared to influence the work reported in this paper.

Data availability

Data will be made available on request.

Acknowledgments

This work was supported by the National Natural Science Foundation of China (NO.42171337) and Beijing Key Laboratory of Urban Spatial Information Engineering (NO.20210210).

References

- [1] T. Oke, G. Mills, A. Christen, J. Voogt, *Urban Climates*, Cambridge University Press, 2017.
- [2] W. Zhou, Y. Tian, Effects of urban three-dimensional morphology on thermal environment: a review, *Acta Ecol. Sin.* 40 (2) (2020) 416–427.
- [3] C. Cao, X. Li, M. Zhang, S. Liu, J. Xu, Correlation analysis of the urban heat island effect and its impact factors in China, *Environ. Sci. J. Integr. Environ. Res.* 38 (10) (2017) 3987–3997.
- [4] C. Grimmond, T.R. Oke, Comparison of heat fluxes from summertime observations in the suburbs of four North American cities, *J. Appl. Meteorol.* 34 (4) (1995) 873–889.
- [5] N. Li, S. Miao, X. Li, J. Dou, Impact of building structure on heat storage flux estimation: an observational case study in Beijing, *Geosci. Rem. Sens. Lett. IEEE* (2020) b) 1–5.
- [6] Y. Liu, Y. Xu, F. Zhang, W. Shu, A preliminary study on the influence of Beijing urban spatial morphology on near-surface wind speed, *Urban Clim.* 34 (2020), 100703.
- [7] X. Zhang, G.-J. Steeneveld, D. Zhou, R.J. Ronda, C. Duan, S. Koopmans, A.A. M. Holtslag, Modelling urban meteorology with increasing refinements for the complex morphology of a typical Chinese city (Xi'an), *Build. Environ.* 182 (2020), 107109.
- [8] Y. Sun, N. Zhang, S. Miao, F. Kong, Y. Zhang, N. Li, Urban morphological parameters of the main cities in China and their application in the WRF model, *J. Adv. Model. Earth Syst.* 13 (8) (2021), e2020MS002382.
- [9] X. He, Y. Li, X. Wang, L. Chen, B. Yu, Y. Zhang, S. Miao, High-resolution dataset of urban canopy parameters for Beijing and its application to the integrated WRF/Urban modelling system, *J. Clean. Prod.* 208 (2019) 373–383.
- [10] S. Shareef, A. Abu-Hijleh, The effect of building height diversity on outdoor microclimate conditions in hot climate, A case study of Dubai-UAE, *Urban Climate* 32 (2020), 100611.
- [11] C. Xi, C. Ren, J. Wang, Z. Feng, S.-J. Cao, Impacts of urban-scale building height diversity on urban climates: a case study of Nanjing, China, *Energy Build.* 251 (2021), 111350.
- [12] Z. Yu, S. Chen, N.H. Wong, Temporal variation in the impact of urban morphology on outdoor air temperature in the tropics: a campus case study, *Build. Environ.* 181 (2020), 107132.
- [13] S. Tong, N.H. Wong, S.K. Jusuf, C.L. Tan, H.F. Wong, M. Ignatius, E. Tan, Study on correlation between air temperature and urban morphology parameters in built environment in northern China, *Build. Environ.* 127 (2018) 239–249.
- [14] Q. Cao, Q. Luan, Y. Liu, R. Wang, The effects of 2D and 3D building morphology on urban environments: a multi-scale analysis in the Beijing metropolitan region, *Build. Environ.* 192 (2021), 107635.
- [15] J. Emery, B. Pohl, J. Crétat, Y. Richard, J. Pergaud, M. Rega, S. Zito, J. Dudek, T. Vairet, D. Joly, T. Thévenin, How local climate zones influence urban air temperature: measurements by bicycle in Dijon, France, *Urban Clim.* 40 (2021), 101017.
- [16] Y. Liu, Q. Li, L. Yang, K. Mu, M. Zhang, J. Liu, Urban heat island effects of various urban morphologies under regional climate conditions, *Sci. Total Environ.* 743 (2020), 140589.
- [17] X. Yang, L. Yao, T. Jin, LL.H. Peng, Z. Jiang, Z. Hu, Y. Ye, Assessing the thermal behavior of different local climate zones in the Nanjing metropolis, China, *Build. Environ.* 137 (2018) 171–184.
- [18] M. Núñez-Peiró, C. Sánchez-Guevara Sánchez, F.J. Neila González, Hourly evolution of intra-urban temperature variability across the local climate zones. The case of Madrid, *Urban Clim.* 39 (2021), 100921.
- [19] R. Du, J. Song, X. Huang, Q. Wang, C. Zhang, O. Brousse, P.W. Chan, High-resolution regional modeling of urban moisture island: mechanisms and implications on thermal comfort, *Build. Environ.* 207 (2022), 108542.
- [20] T. Chen, H. Yang, G. Chen, C.K.C. Lam, J. Hang, X. Wang, Y. Liu, H. Ling, Integrated impacts of tree planting and aspect ratios on thermal environment in street canyons by scaled outdoor experiments, *Sci. Total Environ.* 764 (2021), 142920.
- [21] D. Wang, Y. Shi, G. Chen, L. Zeng, J. Hang, Q. Wang, Urban thermal environment and surface energy balance in 3D high-rise compact urban models: scaled outdoor experiments, *Build. Environ.* 205 (2021), 108251.
- [22] Y. Topalar, B. Blocken, B. Maihue, G.J.F. van Heijst, A review on the CFD analysis of urban microclimate, *Renewable Sustainable Energy Rev.* 80 (2017).
- [23] M. Yu, X. Chen, J. Yang, S. Miao, A new perspective on evaluating high-resolution urban climate simulation with urban canopy parameters, *Urban Clim.* 38 (2021), 100919.
- [24] C. Shen, X. Chen, W. Dai, X. Li, W. Li, Impacts of high-resolution urban canopy parameters within the WRF model on dynamical and thermal fields over Guangzhou, China, *J. Appl. Meteorol. Climatol.* 58 (5) (2019) 1155–1176.
- [25] Z. Li, J. Li, W. Yu, et al., MuSyQ GF-Series 16m/10days Normalized Difference Vegetation Index Product (From 2018 to 2020 across China Version 01), Science Data Bank, 2021.
- [26] J. Zhao, J. Li, Z. Zhang, et al., MuSyQ GF-Series 16m/10days Fractional Vegetation Cover Product (From 2018 to 2020 across China Version 01), Science Data Bank, 2021.
- [27] C. Liang, E. Ng, X. An, R. Chao, M. Lee, U. Wang, Z. He, Sky view factor analysis of street canyons and its implications for daytime intra-urban air temperature differentials in high-rise, high-density urban areas of Hong Kong: a GIS-based simulation approach, *Int. J. Climatol.* 32 (1) (2012) 121–136.
- [28] E. Ng, C. Yuan, L. Chen, C. Ren, J.C.H. Fung, Improving the wind environment in high-density cities by understanding urban morphology and surface roughness: a study in Hong Kong, *Landscape Urban Plann.* 101 (1) (2011) 59–74.
- [29] Y. Yang, C. Cao, X. Pan, X. Li, X. Zhu, Downscaling land surface temperature in an Arid area by using multiple remote sensing indices with random forest regression, *Rem. Sens.* 9 (8) (2017) 789.
- [30] L. Breiman, Random forests, *Mach. Learn.* 45 (1) (2001) 5–32.
- [31] A. Ahmadi, A. Daccache, R.L. Snyder, K. Suvocarev, Meteorological driving forces of reference evapotranspiration and their trends in California, *Sci. Total Environ.* 849 (2022), 157823.
- [32] C. Hutengs, M. Vohland, Downscaling land surface temperatures at regional scales with random forest regression, *Rem. Sens. Environ.* 178 (2016) 127–141.
- [33] S.-Y. Hong, Y. Noh, J. Dudhia, A new vertical diffusion package with an explicit treatment of entrainment processes, *Mon. Weather Rev.* 134 (9) (2006) 2318–2341.
- [34] M.J. Iacono, J.S. Delamere, E.J. Mlawer, M.W. Shephard, S.A. Clough, W. D. Collins, Radiative forcing by long-lived greenhouse gases: calculations with the AER radiative transfer models, *J. Geophys. Res. Atmos.* 113 (D13) (2008).
- [35] G. Thompson, P.R. Field, R.M. Rasmussen, W.D. Hall, Explicit forecasts of winter precipitation using an improved bulk microphysics scheme. Part II: implementation of a new snow parameterization, *Mon. Weather Rev.* 136 (12) (2008) 5095–5115.
- [36] J.S. Kain, J.M. Fritsch, Convective parameterization for mesoscale models: the Kain-fritsch scheme, in: K.A. Emanuel, D.J. Raymond (Eds.), *The Representation of Cumulus Convection in Numerical Models*, American Meteorological Society, Boston, MA, 1993, pp. 165–170.
- [37] F. Chen, D. Jimy, Coupling an advanced land surface-hydrology model with the Penn State-NCAR MM5 modeling system. Part I: model implementation and sensitivity, *Mon. Weather Rev.* 129 (4) (2001) 569–584.
- [38] R.W. Macdonald, R.F. Griffiths, D.J. Hall, An improved method for the estimation of surface roughness of obstacle arrays, *Atmos. Environ.* 32 (11) (1998) 1857–1864.
- [39] C.S.B. Grimmond, T.S. King, M. Roth, T.R. Oke, Aerodynamic roughness of urban areas derived from wind observations, *Boundary-Layer Meteorol.* 89 (1) (1998) 1–24.
- [40] Y. Liu, X. Fang, Q. Luan, Estimation of roughness length of Beijing area based on satellite data and GIS technique, *Plateau Meteorol.* 35 (6) (2016) 1625–1638.
- [41] S.R. Hanna, R.E. Britter, *Wind Flow and Vapor Cloud Dispersion at Industrial and Urban Sites*, John Wiley & Sons Inc, 2002.
- [42] Y. Yuan, C. Li, X. Geng, Z. Yu, Z. Fan, X. Wang, Natural-anthropogenic environment interactively causes the surface urban heat island intensity variations in global climate zones, *Environ. Int.* 170 (2022), 107574.
- [43] P. Potapov, X. Li, A. Hernandez-Serna, A. Tyukavina, M.C. Hansen, A. Kommareddy, A. Pickens, S. Turubanova, H. Tang, C.E. Silva, J. Armston, R. Dubayah, J.B. Blair, M. Hofton, Mapping global forest canopy height through integration of GEDI and Landsat data, *Remote Sens. Environ.* 253 (2021), 112165.
- [44] F. Kong, J. Chen, A. Middel, H. Yin, M. Li, T. Sun, N. Zhang, J. Huang, H. Liu, K. Zhou, J. Ma, Impact of 3-D urban landscape patterns on the outdoor thermal environment: a modelling study with SOLWEIG, *Comput. Environ. Urban Syst.* 94 (2022), 101773.
- [45] I. McRae, F. Freedman, A. Rivera, X. Li, J. Dou, I. Cruz, C. Ren, I. Dronova, H. Fraker, R. Bornstein, Integration of the WUDAPT, WRF, and ENVI-met models to simulate extreme daytime temperature mitigation strategies in San Jose, California, *Build. Environ.* 184 (2020), 107180.